Lasers in Manufacturing Conference 2025

Modeling and analysis of laser drying processes for wet-coated battery electrodes

Teng Chen[a,*], Orçun Atasever[a], Jan-Hendrik Koch[a], Florian Hüsing[a], Christian Brecher[a,b]

[a] *Fraunhofer Institute for Production Technology IPT, Steinbachstraße 17, 52074 Aachen, Germany;*
[b] *Laboratory for Machine Tools and Production Engineering WZL of the RWTH Aachen University, Campus-Boulevard 30, 52074 Aachen, Germany*

Abstract

The drying of lithium-ion battery electrodes is one of the most energy- and cost-intensive processes within the battery production chain. Recently, laser drying has emerged as a promising energy-efficient alternative to the conventional convective and infrared drying methods due to its direct energy input, high energy density and superior controllability. However, the underlying process mechanism remain incompletely understood, and its full potential has yet to be reached. In this work, a numerical process model was developed to simulate the changes in evaporation rates, film thickness as well as the film temperatures, while also estimating the process duration and energy consumption for both laser and convective drying methods. Comparative analysis was made between two drying methods in terms of their process durations and energy consumptions. Furthermore, the process disturbance in the coating and drying processes was addressed, and a concept of model-based process control was developed.

Keywords: laser drying; lithium ion battery; numerical simulation; process control;

1. Introduction

The growing demand for energy storage solutions has firmly established lithium-ion battery (LIB) as a pivotal technology across a wide spectrum of applications, including portable electronics, electric vehicles, and grid-scale energy storage systems (Neb et al. 2022). Among the production chain of LIB electrodes, the coating and drying of the LIB electrodes account for up to 46.8 % of the total energy use, and thus is the most energy-intensive process within the production chain (Liu et al. 2021, p. 3). The state-of-the-industry solution for LIB drying uses convection ovens in a roll-to-roll (R2R) production line. This solution faces various technical challenges, such as low energy efficiency, slow temperature-time response, long process duration, as well as high footprint for drying systems of up to 100 m system length.

In the past few years, laser drying has emerged as one of the promising solutions to the aforementioned challenges due to its ability of generating direct energy input with short reaction time and high spatial precision. Feasibility studies show that the energy consumption of the LIB drying process can be reduced up to 50% by replacing the state-of-the -art convective drying with laser drying solutions. (Vedder et al. 2016, p. 6) So far, laser drying test benches as well as prototype machines have been developed for LIB electrode drying in laboratory scale, but not yet implemented in industrial production. The mechanism of laser-based LIB electrode drying is not fully understood. An adaptive heating process based on the feedback from the process monitoring for such systems has not yet been realized both in laboratory and production environments. In the research project DPP-Open, Fraunhofer IPT has integrated a high-power vertical cavity surface emitting laser (VCSEL) module into a R2R machine and aims to achieve time and space modulation of laser radiation in R2R LIB laser drying processes. To realize the adaptive process control, a process model is necessary to gain deeper understanding about the

* Corresponding author. Tel.: +49 241 8904-473; fax: +49 241 8904-6473.
E-mail address: teng.chen@ipt.fraunhofer.de

laser drying process. In the present work, a numerical model is established, and a model-based parameter study is conducted for both laser and convective drying.

2. State of the art

2.1. Mechanism and modelling of lithium-ion battery electrode drying

The manufacturing of LIB electrodes includes following process steps: mixing, coating, drying, calendering, slitting and vacuum drying. (Heimes et al. 2018)During the coating process, the wet electrode film is applied to a metallic current collector foil by slot-die coating. The film of LIB anode electrodes is typically a slurry consisting of graphite as active material, carbon black as conductive additive, carboxymethyl cellulose (CMC) as binder and water as the solvent. (Park et al. 2023, p. 2) The following drying process then removes the solvent from the coated film and solidifies the film layer. In the industrial production, the convective method is widely used for LIB electrode drying. In this method, the hot air flow is applied onto the wet film and serves on the one hand as the energy source to heat up the film and accelerate the diffusion of the solvent particles, and on the other hand as the medium to carry away the evaporated solvent particles from the process zone. This leads to a coupling of the heat and mass transfer process and thus limits the heat transfer efficiency and process flexibility.

The drying mechanisms for LIB electrodes can be summarized into multiple stages. At the drying process start, i.e. directly after the coating, particles of active materials and binders are suspended in the solvent with a homogeneous material distribution. As the drying process begins, the solvent is evaporated from the film surface, causing the film consolidation and subsequently the shrinkage of the film thickness. In this stage, a constant evaporation rate can be achieved at constant process parameters. In the second stage, the wet film is consolidated into semi-slurry form, and the film stops shrinking. The evaporation rate remains constant at this stage. As the process progresses into the third stage, the active material consolidates further and forms a porous structure, and the solvent is evaporated from the internal interfaces of the film instead of on the surface. Subsequently solvent vapor has to be transported to the surface via diffusion processes At this stage a non-linearly decreasing evaporation rate is observed until the end of the drying process. (Zhang et al. 2022) When observing the evaporation rate and the residue solvent concentration, the drying process is described in two phases by merging the first two stages into the first phase, the constant rate phase (CRP) and the third stage as the second phase, the decreasing rate phase (DRP). Experiments show that up to 90% of the solvent is evaporated within the CRP. (Jaiser et al. 2016) Due to this fact the CRP phase is particularly suitable for increase in evaporation rates due to laser usage.

Different studies have developed process models to describe the LIB electrode drying process. It is common to model the CRP and DRP separately, as different mechanisms determine the drying process in different phases. Oppegård et al. developed a one-dimensional numerical model to describe the change of temperature and the solvent concentration of a convective drying process, assuming that all drying process happens under CRP phase conditions. (Oppegård et al. 2021) Susarla et al. developed a numerical model focusing on the DRP drying, and discovered that a multi-stage convection drying, in which the electrodes sequentially go through three ovens with different air temperature settings, which reduces the total energy consumption by up to 50%. (Susarla et al. 2018)

In summary, despite the process optimization of in convection drying process, the drying method faces multiple technical limitations, including low energy efficiency, long process duration, high spatial footprint due to long heating length, and limited flexibility in process parameterization due to the coupled heat and mass transfer through hot air. Additionally, the drying process is not robust against process disturbances resulting from previous coating process, typically inhomogeneous film thickness and varying local solvent concentrations. Therefore, an alternative drying method is required to solve these problems. Therefore, the use of laser radiation is investigated within this paper.

2.2. Laser drying of lithium-ion battery electrode

Laser drying is one of the most promising technical alternatives to the conventional convective drying that has been investigated in recent years. (Horstig et al. 2022) Compared to the convective drying method, laser drying benefits from its direct energy input with high intensity through laser radiation, which minimizes the energy waste in heating up the environment and reduces the space requirements for the drying process by shortening the necessary length for equal energy input. Moreover, the use of laser radiation as the heat source decouples the heat and mass transfer processes and improves the process flexibility. Convection is expected to be used in parallel to laser drying in order to remove solvent efficiently. Furthermore, the controllability and high time and space precision of the laser module also enables the control of local intensity, mitigating the problem of inhomogeneous drying caused by convective drying methods. (Wolf et al. 2023, pp. 1–2)

Several studies have investigated the laser drying of LIB electrodes. Vedder et al. developed a scanning-based laser drying process, where the laser source is combined with a scanner to realize high-speed scanning of the laser spot on the water-based electrode slurries. The electrode samples showed comparable mechanical and electrochemical properties with the ones processed via convective drying, while the energy-consumption of the laser drying process is about 50% lower than convective method. However, electrode defects due to high local intensity were observed on the laser-dried samples. (Vedder et al. 2016) In another study, vertical-cavity surface-emitting lasers (VCSEL) equipped with zoom optics were used to generate a homogeneous laser radiation zone with lower intensity. (Neb et al. 2022) Wolf et al. integrated a diode laser module into a R2R convection oven and realized a hybrid drying process, where the film was dried by laser radiation, and then via convection. (Wolf et al. 2023)

So far, the feasibility of laser-based LIB electrode drying has been proven but its full potential remains unexplored. Compared to the state-of-the-art solution with multi-stage convection oven, the usage of laser radiation offers more flexibility in defining the temperature profile. However, deeper understanding of the drying process under laser radiation is necessary to develop a sophisticated laser drying strategy for electrodes. Within this work, a numerical process model is developed to describe the CRP of the drying process.

3. Modelling methodology

3.1. Model description

A numerical, one-dimensional model is built to describe the process during the laser-based electrode drying process, focusing on the heat and mass transfer within the wet film in CRP. The setup of the model is illustrated in Fig. 1. The wet film is applied on one side of the substrate and is considered as a binary system consisting of water as solvent (s) and graphite as active material particles (p). Binders and conductive additives are ignored due to their low concentration (< 5 wt% in total). A laminar air flow with constant air velocity v and air temperature T_a is applied on top of the wet film. The process starts with a homogeneous initial film temperature T_0 and initial solvent mass concentration C_0. The mass and heat transfer between the wet film and the environment happens at the film-air interface defined in Fig. 1. The solvent particles evaporate at the film-air interface and enter the gas phase in the form of solvent vapor. Through the energy exchange at the same interface, the wet film is heated up by a combined effect from laser radiation and forced convection of the air flow. Due to the small film thickness, the heat and mass transfer within the film is neglected, and the film temperature as well as the solvent mass concentration are considered homogeneous along the thickness direction of the film.

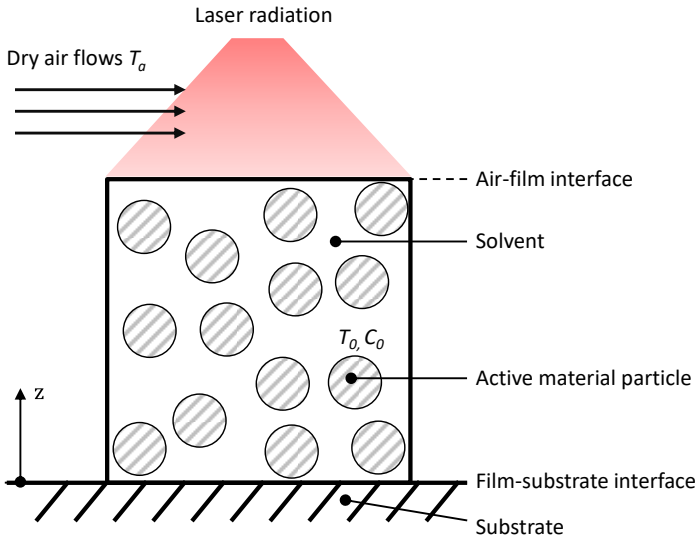

Fig. 1 Model setup for the drying process for lithium-ion battery electrodes

To simplify the calculation while ensuring a mathematically manageable model, the following assumptions are made for the drying process:

1. The laser radiation is absorbed at the top surface of the film due to the low penetration depth of laser radiation in graphite (0.15 µm).
2. The material properties of all compositions such as solvent, binder and active materials, including density, heat capacity, heat transfer coefficient and the absorbility in laser wavelength, are considered as constant across the

temperature range. The overall material properties of the film depend on mass concentration of the solvent and the active material.

3. Ideal gas law applies to both the air and the solvent vapor in the model.
4. The film-substrate interface is considered adiabatic and impenetrable.
5. Gravitational effects are negligible due to the small thickness of the film.

Three key time-dependent variables, namely film temperature, evaporation rate as well as solvent concentration are determined as key process indicators and will be used for process analysis in Chapter 4.

3.2. Mathematical derivation

The drying process is governed by a coupled heat and mass transfer process. The two governing equations of the system considering its energy and mass balances within the film are given as equations (1) and (2) respectively.

$$\frac{dT}{dt} = \frac{\dot{q}_{conv} + \dot{q}_{laser} - \dot{m}_{evap} \cdot H_v}{\rho_f \cdot C_{p,f} \cdot h} - \frac{T}{h}\frac{dh}{dt} - \frac{T}{\rho_f}\frac{d\rho_f}{dt} - \frac{T}{C_{p,f}}\frac{dC_{p,f}}{dt} \quad (1)$$

$$\rho_f \frac{dh}{dt} = \dot{m}_{evap} - h \cdot \frac{d\rho_f}{dt} \quad (2)$$

T denotes the film temperature, while $\dot{q}_{conv}$ and $\dot{q}_{laser}$ indicates the total input heat flux introduced by convective air flows and by laser radiation, respectively; $\dot{m}_{ev}$ represents the evaporation rate; $\mathrm{H_v}$ is the latent heat of the solvent vapor; ρ_f denotes the overall density of the film; $C_{p,f}$ is the overall heat capacity of the film; h is the film thickness.

The value of $\dot{q}_{conv}$ is calculated through:

$$\dot{q}_{conv} = k_c \cdot (T_a - T) \quad (3)$$

where k_c is the convective heat transfer coefficient under the laminar air flow, and T_a denotes the air temperature.

Based on the adiabatic boundary condition of the top surface and the ideal gas law, the value of the evaporation rate $\dot{m}_{ev}$ can be calculated as follows:

$$\dot{m}_{ev} = \frac{k_m \cdot M_s}{R}\left(\frac{P_s}{T_s} - \frac{P_a}{T_a}\right) \quad (4)$$

where k_m is the mass transfer coefficient; M_s is the molecular weight of the solvent particles; R is the ideal gas constant; P_s and P_a are the partial pressures of solvent vapor and of air; T_s is the temperature of the solvent vapor.

The value of k_c can be estimated by the empirical equation as follows (Susarla et al. 2018, p. 667):

$$k_c = 0.037 \cdot V_a^{0.8} \cdot \left(\frac{\mu_a}{\rho_a}\right)^{-0.8} \cdot Pr^{\frac{1}{3}} \cdot \lambda_a \cdot L^{-0.2} \quad (5)$$

where V_a is the air velocity, μ_a is the air dynamic viscosity, ρ_a is the air density, Pr is the Prandtl number, λ_a is the thermal conductivity of air and L is the characteristic length of the drying area.

Based on the Chilton-Colburn correlation, the value of mass transfer coefficient can be estimated by (Chilton and Colburn 1934):

$$k_m = \frac{k_c}{\rho_a \cdot C_{p,a}} \cdot Le^{-2/3} \quad (6)$$

where C_{pa} is the heat capacity of the air, and Le is the Lewis number. The two dimensionless numbers Pr and Le are defined as follows:

$$Pr = \frac{C_{p,a} \cdot \lambda_a}{\mu_a} \tag{7}$$

$$Le = \frac{\lambda_a}{C_{p,a} \cdot \rho_a \cdot D_a} \tag{8}$$

where D_a is the mutual diffusion coefficient between solvent vapor and air.

For water-based solvent, the latent heat of the vaporization can be approximated by a second-degree polynomial function of film temperature T (Oppegård et al. 2021, p. 79):

$$\lambda = -3.345 \cdot T^2 - 259.3 \cdot T + 2.817 \cdot 10^6 \tag{9}$$

The overall film density ρ_f as well as the overall heat capacity of the film $C_{p,f}$ are determined by the mass concentration of solvent C_s:

$$\rho_f = \frac{\rho_s \cdot \rho_p}{\rho_s \cdot C_p + \rho_p \cdot C_s} \tag{10}$$

$$C_{p,f} = C_{p,s} \cdot C_s + C_{p,p} \cdot (1 - C_s) \tag{11}$$

The partial pressure of the the solvent flow P_s can be estimated using Flory-Huggins theory (Khansary 2016, p. 1402):

$$P_s = P_0 \, exp\left[\chi \cdot \phi_p^2 + ln(\phi_s) + \left(1 - \frac{\hat{V}_s}{\hat{V}_p}\right)\phi_p\right] \tag{12}$$

where P_0 is the pure solvent pressure, χ is the Flory-Huggins interaction parameter and $\hat{V}_s$ and $\hat{V}_p$ represents the molar volumes of solvent and active material particles, respectively. The pure solvent pressure is calculated based on the Antoine equation for saturated vapor pressure (DDBST GmbH 2023):

$$P_0 = 133.332 \cdot 10^{8.07131 - \frac{1730.63}{233.426 + T}} \tag{13}$$

Similarly, the partial pressure of air can be determined as follows:

$$P_a = \varphi \cdot 133.332 \cdot 10^{7.54826 - \frac{1979.68}{222.2 + T_a}} \tag{14}$$

where φ is the relative humidity of the air flow. Combining governing equations (1) and (2) with all supporting equations (3) – (14), the time-dependent film temperature as well as the film thickness can be determined.

3.3. Parameter settings

The mathematical model is discretized using finite difference method and is implemented in MALTAB®. Water and graphite are chosen as solvent and active materials, and their material properties are used in the drying simulation. The process parameters as well as initial conditions are given in Table 1. To compare the performance between convection and laser drying, two parameter sets are used for the simulation. For laser drying only, an air flow with constant air velocity at room temperature (20 °C) is used to guarantee the solvent mass transfer. For convection drying, the air flow is modelled with an elevated temperature (140 °C) and no laser intensity is applied.

The energy consumptions of laser and convective drying processes were calculated and compared to each other. For the laser drying, an electro-optical efficiency of 50% was used to calculate the energy consumption. This value is obtained from the specification of the existing VCSEL module at Fraunhofer IPT, produced by TRUMPF Photonic Components GmbH. For the convective drying, an air flow volume of 30.2 L/min was used based on the assumption for a material band width of

1 m. The air flows are heated up to the process temperature before entering the drying process zone. The comparison between convective and laser drying is shown in Section 4.1.

Table 1. Process parameters for drying simulations

Description	Symbol	Value	Unit
Air velocity	V_a	10	m/s
Air temperature	T_a	20 (laser); 140 (convection)	°C
Laser intensity	$\dot{q}_{laser}$	1.68 (laser); 0 (convection)	W/cm²
Initial film thickness	h_0	160	µm
Initial film temperature	T_0	20	°C
Initial solvent mass concentration	$C_{s,0}$	55	%

Another parameter study is conducted to investigate the effect of process disturbance on the laser drying process. Two disturbance factors coming from the previous slurry preparation and the coating process, namely the initial coating thickness h_0 and initial solvent concentration $C_{s,0}$, are chosen as the observed parameters for a sensitivity analysis. For the varying initial coating thickness, varying initial thickness values ranging from 145 µm to 175 µm were selected for the simulation. Similarly, the initial solvent mass concentration varying from 50 % to 60 % were simulated. The results and analysis of the process disturbance is shown in Section 4.2.

4. Results and discussion

4.1. Comparison between convective and laser drying

The changes of temperature, solvent concentration as well as film thickness over time are shown in Fig. 2. All simulation results show a three-stage temperature response during drying. As the drying process begins, the film is heated up rapidly by convective air flow or laser radiation, and the film temperature rises the rapid heating stage (RH). At the end of RH, the film temperature reaches a quasi-steady state, and the evaporation rate stays constant. This stage is therefore named as quasi-steady-state stage (QSS). As the evaporation proceeds, the solvent concentration reduces steadily, causing a stable and gradual change of the overall film material properties. At the final stage, the evaporation rate decreases, causing a milder change in the film thickness. Meanwhile, the temperature rises again at the final overheating stage (OH), which has to be avoided. The three-stage temperature change is also observed during the laser drying experiment, and the trend is consistent with the simulation results shown in Wolf et al. (Wolf et al. 2023, p. 4).

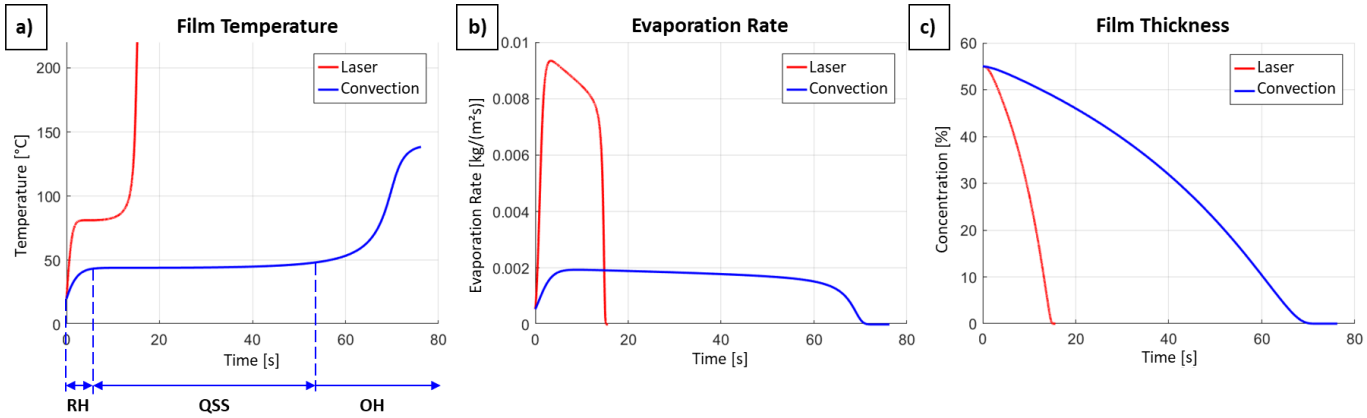

Fig. 2 Simulated changes of a) film temperature, b) evaporation rate, and c) solvent concentration during the laser and convection drying process

Due to the higher energy flux, the drying process induced by laser radiation reaches the QSS stage within a shorter period, compared to the convective drying case. Moreover, a higher quasi-steady-state temperature can be reached by laser drying than that by convective drying, which results in a higher evaporation rate during the second stage. Both factors lead to a 79.5% shorter process duration in the laser drying process, compared to that in the convection process.

As shown in Table 2, the total energy consumption of the drying process is 75% lower than the convective drying. The reasons for the significant difference are a significantly shortened process duration and improved energy efficiency. The nature of direct energy input of the laser radiation and the high absorptivity of the slurry (up to 90%) in the near infrared laser wavelength leads to an optimal absorption of laser radiation by the slurry and a minimized energy waste in heating up the environment. Despite the approximately 50% electro-optical efficiency of the laser source, the overall energy efficiency is still significantly higher than the convection drying case (without heat recuperation), in which little proportion of heat energy is converted from the heated air flow into the slurry.

Table 2. Process parameters for drying simulations

	Laser	Convection
Process duration [s]	15.6	76.2
Energy consumption [kJ/m²]	2917	11594

The high energy input in laser drying also leads to a more drastic temperature rise in the OH stage, which may result in quality problems such as cracks and delamination in real drying trials. It is therefore suggested to apply the laser radiation only in the first two stages in the first two stages to accelerate the drying process, while use milder laser radiation or heated air flow to proceed the drying in order to avoid the overheating of the film and its resulting quality problems like crack formation. The challenge is expected to be the real-time detection of the end of the QSS phase during the drying process.

4.2. Temperature response sensitivity analysis for process disturbances

The temperature profiles of the drying process under varying initial film thicknesses and solvent mass concentrations are plotted in Fig. 3 a) and b) respectively. It is observed that varying the initial film thickness leads to the change of heating rates and the duration of the RH stage, while has little effect on the quasi-steady state temperature. Thinner films exhibit slightly higher temperature with a faster heating. The thickness variation also affects the ending time of the QSS stage and therefore the total process duration.

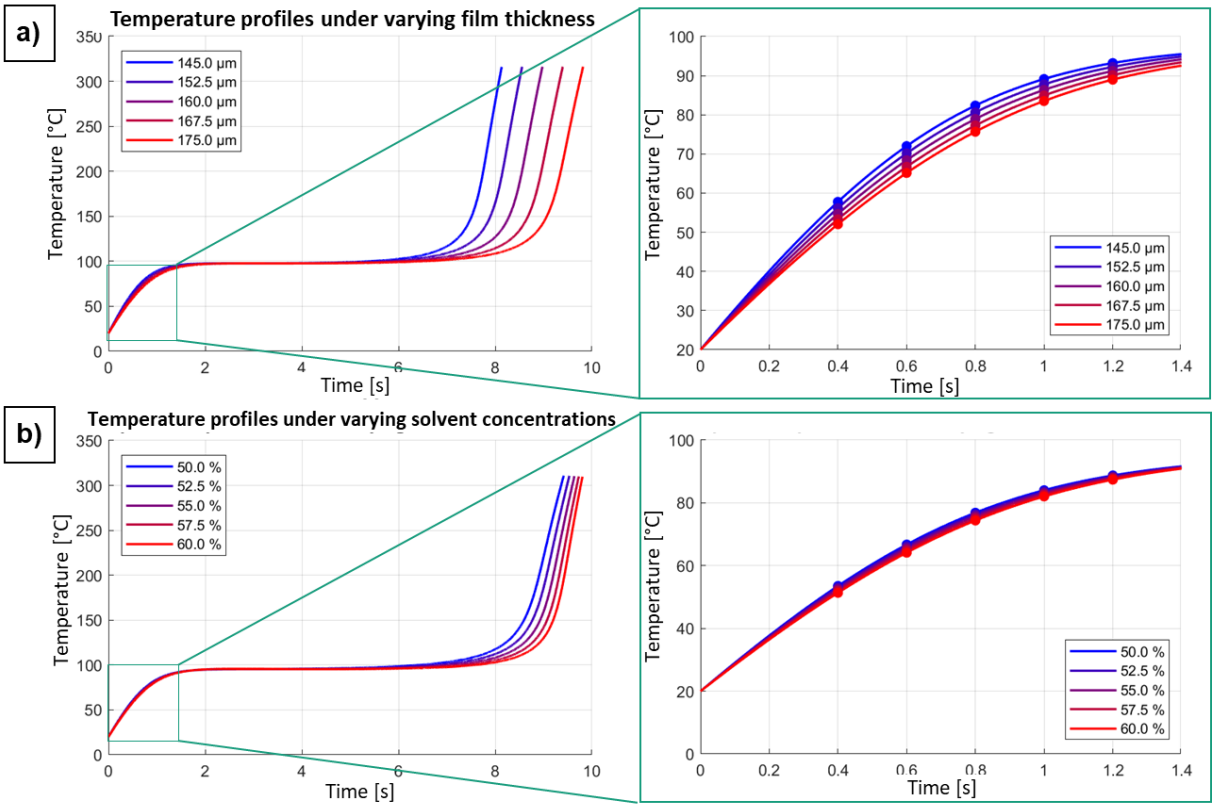

Fig. 3 Temperature responses under varying a) initial film thicknesses and b) solvent mass concentrations.

To quantify the temperature difference in the RH stage, the temperature values at five discrete and equidistant observing time points within the first 1.2 second are chosen. The temperature difference over time increases during the first 0.8 second, then decreases as all profiles converge into the quasi-steady stage temperature. At the time point t = 0.8 s, the variation of the initial film thickness by 15 µm from the reference thickness (160 µm) results in a temperature deviation of up to 3.4 K, and a 7.5 µm variation in film thickness results in a temperature deviation of up to 1.7 K. This temperature deviation can be observed by a contactless temperature measurement device, e.g. an industrial infrared camera or pyrometers, the measurement accuracy of which lies typically at 1 K or below if special calibration methods are applied. The correlation between the thickness and temperature deviation shows a linear trend within the observation time range.

In comparison, the variation of initial concentration by ±5% from the reference concentration of 55% leads to insignificant temperature fluctuation of up to 0.5 K and the process duration is influenced less than in the first case (see Fig. 3 b). To summarize the sensitivity analysis, the coating thickness variation affects the drying process more and can be detected by measuring the temperature profile during the drying process or the film thickness before the drying process. Furthermore, a linear correlation between the initial film thickness and the temperature deviation is observed within the investigate variation range. This enables the indirect control of the drying process by controlling the temperature profiles.

4.3. Concept of temperature-based drying process control

Based on the correlation found between the initial coating thickness and the temperature profiles, a concept of temperature-based process optimization was developed. The concept is based on compensating the varying coating thickness in the width direction of the material band by detecting the local initial thickness and scale the local laser intensity according to the temperature deviation. To verify the concept, simulations are conducted under different initial coating thicknesses with scaled laser intensity. As shown in Fig. 4, the temperature profile deviation is reduced after the process optimization, and the effect is propagated to the concentration profiles. The maximum deviation of the concentration

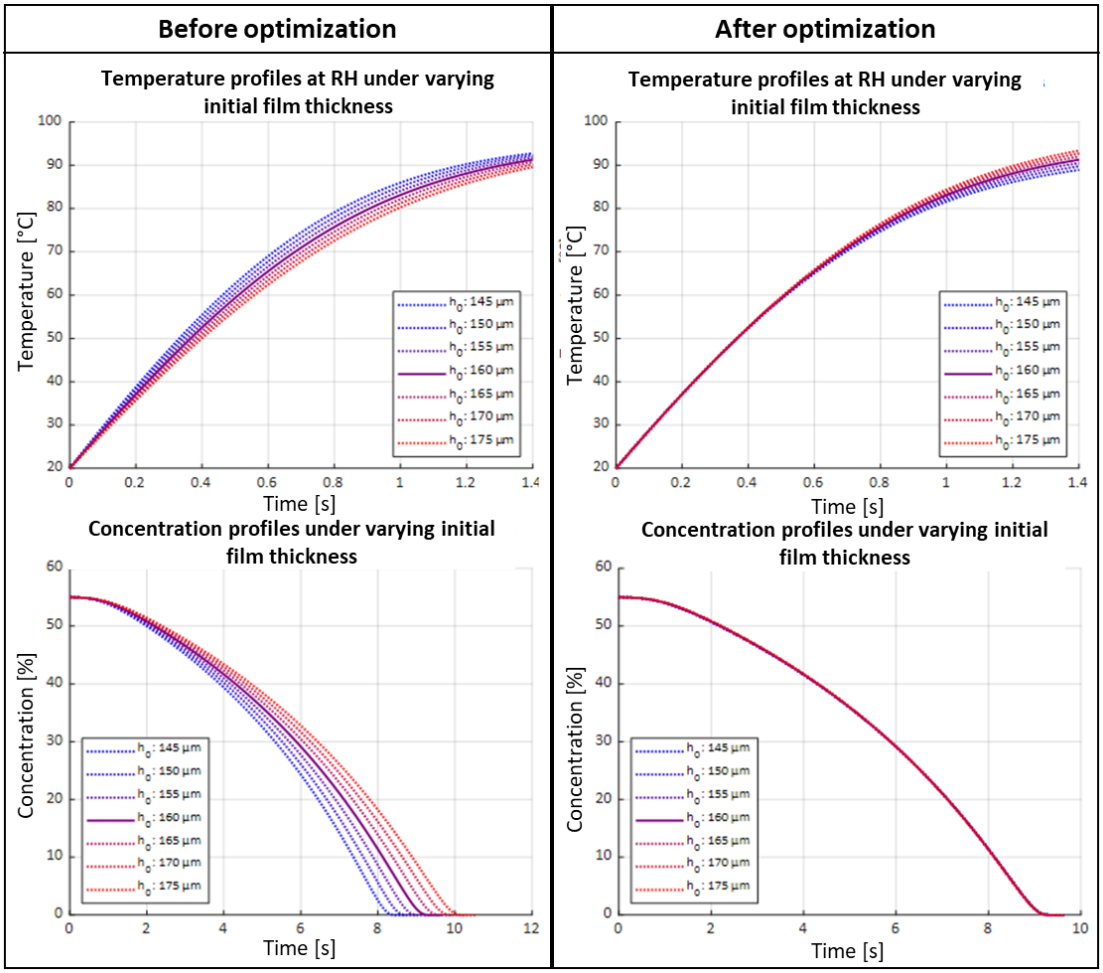

Fig. 4. Temperature and concentration profiles before (left) and after implementing process optimization (right)

profiles is reduced significantly from up to 10% to 0.05%, and the drying process ends almost simultaneously under different initial film thickness. This suggests the feasibility of a temperature-based drying process control.

In the real production processes, a gradient film thickness in the width direction of the film can result from the imperfect positioning of the coating unit as well as the oscillation of the material movement. Through the combination of temperature-based process control and a locally adjustable laser input, an improvement in the process robustness can be reached, and a more homogeneous temperature distribution is expected to be achieved. The left half of Fig. 5 illustrates a R2R system setup that enables the implementation of this control. A high-power VCSEL laser module developed by Trumpf Photonic Components GmbH is installed on top of a coated electrode material band with constant web speed. The multiple emitters of the VCSEL module are arranged perpendicular to the material feed direction, enabling a local adjustment of laser energy inputs along the material's width direction.

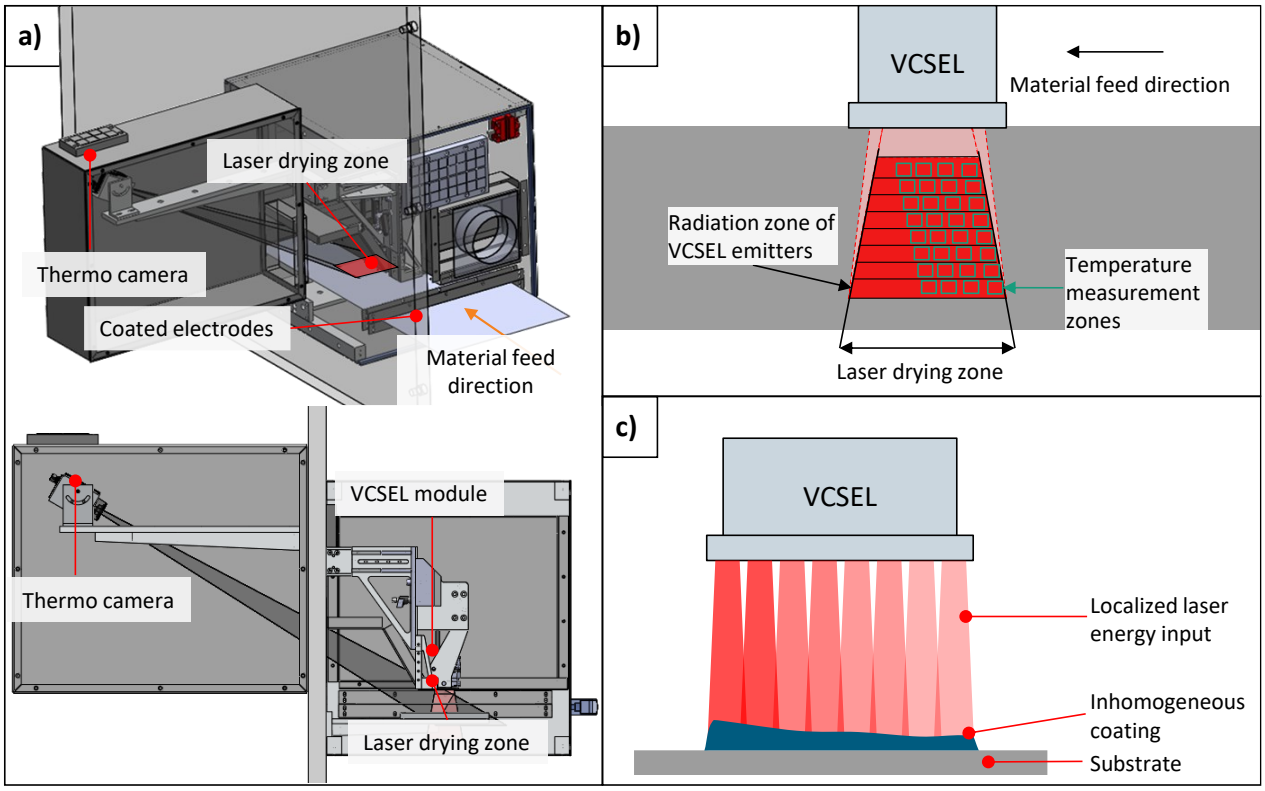

Fig. 5. a) System concept for a temperature-based drying process control; b) Temperature measurement zones in the camera image; c) Localized laser energy input.

The real-time temperature response of the film can be obtained by an infrared camera. By defining multiple measurement zones along the material feed direction below one laser emitter, the local temperature response can be recorded as it can be seen in Fig. 5 b). The output power of the emitter above measurement zones is adjusted by the controller to realize a targeting temperature response, as shown in Fig. 5 c). Combining these techniques to all VCSEL emitters, a temperature-based, adaptive energy input can be realized and is expected to compensate the drying inhomogeneity caused by the imperfect coating process.

5. Summary, conclusions and outlooks

This study has developed a numerical model to describe the laser drying process of LIB electrodes and has conducted a model-based case study to compare the performance of laser and convection drying process. Additionally, a model-based sensitivity analysis was conducted to determine the effect of two disturbance factors out of the previous coating process, the variation in coating thickness and the solvent concentration. Main conclusions are found as follows:

1. The application of laser drying has the potential to shorten the drying process duration by up to 79.5% and reduce the process energy consumption by up to 75%, compared to the state-of-the art convection drying method. To avoid overheating of the film, the application of high laser radiation (>1.6 W/cm²) is suggested only in the first two stages.

2. The temperature profile can be used as an indicator to determine the initial film thickness during the continuous process. A concept was established that enables the implementation of a temperature-based drying process control. The concept is expected to reach a more homogeneous drying quality even with inhomogeneous coating process inputs.

The implementation of the control concept into the R2R test bench as well as a verification test of the control concept are planned as the next step at Fraunhofer IPT.

Acknowledgements

This research is a combined contribution in two research projects:

1. The process modelling part is a contribution in the research project *Research campus Digital Photonic Production Open-Know-how-Pool (DPP-Open),* funded by German Federal Ministry of Research, Technology and Space (BMFTR), project number 13N15424.

2. The concept development for temperature-based control is a contribution in the research project *Thermoplastic mono-material sandwich materials optimized for the circular economy* (TherMono), funded by Federal Ministry for Economic Affairs and Energy (BMWE), project number 03LB2081A.

References

Chilton, T. H.; Colburn, A. P. (1934): Mass Transfer (Absorption) Coefficients Prediction from Data on Heat Transfer and Fluid Friction. In *Ind. Eng. Chem.* 26 (11), pp. 1183–1187. DOI: 10.1021/ie50299a012.

DDBST GmbH (2023): Saturated Vapor Pressure of Water. DDBST GmbH. Available online at http://ddbonline.ddbst.de/AntoineCalculation/AntoineCalculationCGI.exe?component=Water, checked on 5/2/2025.

Heimes, Heiner Hans; Kampker, Achim; Lienemann, Christoph; Locke, Marc; Offermanns, Christian; Michaelis, Sarah; Rahimzei, Ehsan (2018): Lithium-ion battery cell production process. Aachen, Frankfurt am Main: PEM der RWTH Aachen University; DVMA. Available online at http://www.pem.rwth-aachen.de/global/show_document.asp?id=aaaaaaaaabdqbtk.

Horstig, Max-Wolfram von; Schoo, Alexander; Loellhoeffel, Thomas; Mayer, Julian K.; Kwade, Arno (2022): A Perspective on Innovative Drying Methods for Energy-Efficient Solvent-Based Production of Lithium-Ion Battery Electrodes. In *Energy Tech* 10 (12), p. 2200689. DOI: 10.1002/ente.202200689.

Jaiser, Stefan; Müller, Marcus; Baunach, Michael; Bauer, Werner; Scharfer, Philip; Schabel, Wilhelm (2016): Investigation of film solidification and binder migration during drying of Li-Ion battery anodes. In *Journal of Power Sources* 318, pp. 210–219. DOI: 10.1016/j.jpowsour.2016.04.018.

Khansary, Milad Asgarpour (2016): Vapor pressure and Flory-Huggins interaction parameters in binary polymeric solutions. In *Korean J. Chem. Eng.* 33 (4), pp. 1402–1407. DOI: 10.1007/s11814-015-0277-6.

Liu, Yangtao; Zhang, Ruihan; Wang, Jun; Wang, Yan (2021): Current and future lithium-ion battery manufacturing. In *iScience* 24 (4), pp. 1–17. DOI: 10.1016/j.isci.2021.102332.

Neb, Daniel; Kim, Stanislav; Clever, Henning; Dorn, Benjamin; Kampker, Achim (2022): Current advances on laser drying of electrodes for lithium-ion battery cells. In *Procedia CIRP* 107, pp. 1577–1587. DOI: 10.1016/j.procir.2022.05.194.

Oppegård, Emil; Jinasena, Asanthi; Hammer Strømman, Anders; Are Suul, Jon; Stokke Burheim, Odne (2021): Study of an Industrial Electrode Dryer of a Lithium-Ion Battery Manufacturing Plant: Dynamic Modeling. In : Proceedings of The 61st SIMS Conference on Simulation and Modelling SIMS 2020, September 22-24, Virtual Conference, Finland. SIMS Conference on Simulation and Modelling SIMS 2020, September 22-24, Virtual Conference, Finland, 2020-09-22: Linköping University Electronic Press (Linköping Electronic Conference Proceedings), pp. 77–84.

Park, Jeong Hoon; Kim, Sun Hyung; Ahn, Kyung Hyun (2023): Role of carboxymethyl cellulose binder and its effect on the preparation process of anode slurries for Li-ion batteries. In *Colloids and Surfaces A: Physicochemical and Engineering Aspects* 664, p. 131130. DOI: 10.1016/j.colsurfa.2023.131130.

Susarla, Naresh; Ahmed, Shabbir; Dees, Dennis W. (2018): Modeling and analysis of solvent removal during Li-ion battery electrode drying. In *Journal of Power Sources* 378, pp. 660–670. DOI: 10.1016/j.jpowsour.2018.01.007.

Vedder, Christian; Hawelka, Dominik; Wolter, Mareike; Leiva, Diana; Stollenwerk, Jochen; Wissenbach, Konrad (2016): Laser-based drying of battery electrode layers. In : International Congress on Applications of Lasers & Electro-Optics. ICALEO® 2016: 35th International Congress on Applications of Lasers & Electro-Optics. San Diego, California, USA, October 16–20, 2016: Laser Institute of America, N501.

Wolf, Sebastian; Schwenzer, Niklas; Tratz, Tim; Göken, Vinzenz; Börner, Markus; Neb, Daniel et al. (2023): Optimized LiFePO4-Based Cathode Production for Lithium-Ion Batteries through Laser- and Convection-Based Hybrid Drying Process. In *WEVJ* 14 (10), p. 281. DOI: 10.3390/wevj14100281.

Zhang, Ye Shui; Courtier, Nicola E.; Zhang, Zhenyu; Liu, Kailong; Bailey, Josh J.; Boyce, Adam M. et al. (2022): A Review of Lithium-Ion Battery Electrode Drying: Mechanisms and Metrology. In *Advanced Energy Materials* 12 (2), p. 2102233. DOI: 10.1002/aenm.202102233.